Microporous Membranes

International Edition: DOI: 10.1002/anie.201508367
German Edition: DOI: 10.1002/ange.201508367

In situ Generation of Reticulate Micropores through Covalent Network/Polymer Nanocomposite Membranes for Reverse-Selective Separation of Carbon Dioxide

*Eunkyung Jeon, Su-Young Moon, Jae-Sung Bae, and Ji-Woong Park**

Abstract: *We demonstrate the synthesis of a microporous covalent-network membrane derived from co-continuous blends of a porogenic urea network and a polyimide (PI). We show that the urea networks in the PI matrix may be thermally rearranged while selectively expelling small molecular fragments, thereby forming a new network bearing reticular microporous molecular pathways. The porous structures enable reverse-selective gas separation, efficiently blocking carbon dioxide to which most polymeric membranes exhibit selective permeability. The proposed method for fabricating microporous organic membranes with highly tunable porosities using a variety of chemical structures and processing parameters is facile and shows promise for the creation of new membrane-based molecular-separation techniques.*

Covalent molecular networks with micropores,[1] defined according to IUPAC as having a pore width under 2 nm, show promise for molecular separation and storage,[2] as catalysts,[3] or catalyst-support[4] materials. Several molecular-scale organic network materials have been developed, including crystalline networks, such as covalent organic frameworks (COFs),[5] metal–organic frameworks (MOFs),[6] and amorphous networks, such as polymers with an intrinsic microporosity (PIMs),[7] porous polymer networks (PPNs),[3b,8] conjugated microporous polymers (CMPs),[9] or hypercrosslinked polymers (HCPs).[10] These network materials, either crystalline or amorphous, tend to be poorly processable owing to their inherent insolubility and infusibility and, thus, used mainly as gas or liquid adsorbents in their powdery form. Methods that could facilitate the fabrication of different shapes, such as beads, sheets, films, or monoliths, while maintaining their porous properties,[11] could lead to the broader application of microporous networks.

Membrane-based molecular separation applications require preparation of defect-free films on a large area; however, this has proven to be challenging with the insoluble network materials. Only a limited number of approaches have yielded covalent-network films that provide membrane-like transport properties.[12] Furthermore, a film of a dense covalent network would provide a gas permeability that is too low for use in practical applications. Instead of preparing dense microporous network membranes, microporous particles may be deposited onto a porous polymer support.[13] In this method, the gaps between the crystalline grains must be sealed by thermal or chemical treatment and, in many cases, a crystalline layer must be deposited thick enough to eliminate the pinholes that reduce the separation selectivity. Mixed matrix membranes (MMM) composed of microporous particles dispersed in a polymer matrix have also been developed as microporous membranes.[14] Unfortunately, poor distributions of the particles and the weak interfacial contact between particle and polymer matrix can generate defects that reduce the membrane performance.[14c]

Herein, we describe the synthesis of a new type of microporous membrane composed of a pore-generating (porogenic) organic molecular network and a polymer, which together form a three-dimensional interpenetrating microphase via phase-separation. Reticulated channels of micropores were then generated in situ across the covalent-network domain in the blend via thermal rearrangement resulting in expulsion of small-molecule fragments. The resultant polymer membranes formed continuous through-micropores that exhibit unusual reverse selectivity (carbon dioxide rejection and nitrogen transport). The facile method for fabricating the reverse-selective microporous membranes with porosities that can be tuned using different combinations of blended components and the processing parameters for pore generation shows promise for the creation of new membrane-based molecular separation techniques.

Urea bonds can dissociate to form the corresponding amine and isocyanate at temperatures above 200 °C.[15] The chemistry of urea bonds was recently used to show that molecularly crosslinked covalent networks consisting of urea bonds could be rearranged to form a rigid framework while generating reticulated micropores.[16] We envisaged that if these porogenic networks could be embedded within a thin polymer film to form a continuous microdomain, subsequent thermal treatment could generate continuous molecular channels across the flexible composite film (Figure 1). A prerequisite to this idea involves the preparation of a nanocomposite polymer film containing three-dimensional co-continuous nanoscale domains of the porogenic urea network and a matrix polymer.

To obtain the blends of the urea-based network (UN) and a polymer (Figure 1) that phase-separated into continuous microdomains, we first synthesized UN nanoparticle sols by polymerizing a multifunctional amine and an isocyanate as reported recently.[12a–c] The sol state of nano-parituclate UNs

[*] E. Jeon, Dr. S.-Y. Moon, J.-S. Bae, Prof. J.-W. Park
School of Materials Science and Engineering
Gwangju Institute of Science and Technology
123 Cheomdan-gwagiro, Buk-gu, Gwangju, 61005 (Korea)
E-mail: jiwoong@gist.ac.kr

Supporting information and ORCID(s) from the author(s) for this article are available on the WWW under http://dx.doi.org/10.1002/anie.201508367.

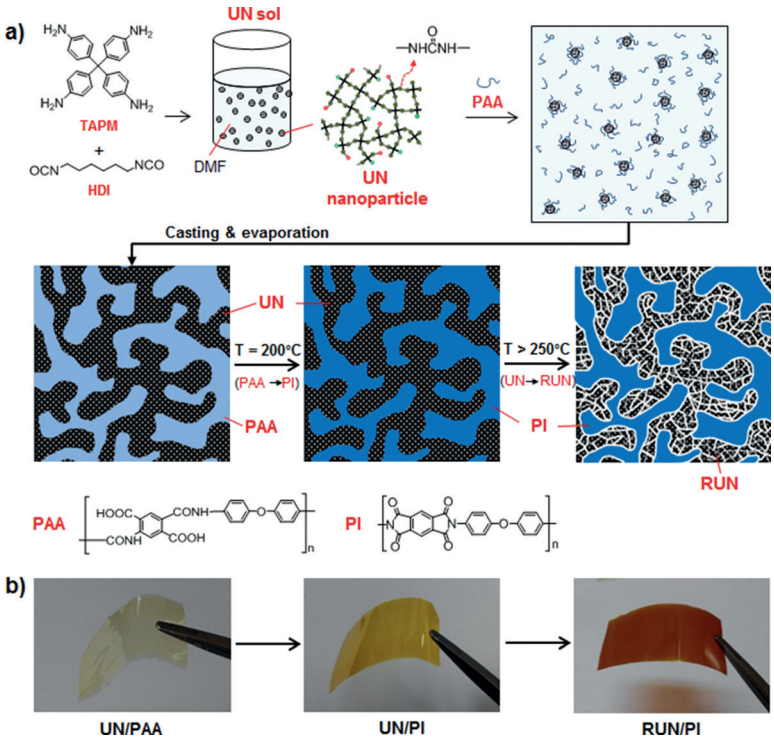

Figure 1. a) Schematic illustration of the experimental procedure used to fabricate microporous membranes through thermal rearrangement of the porogenic network in the polymer matrix. A urea-based network (UN) sol is first prepared by cross-linking polymerization below a critical gelation point, to which PAA solution is added. Subsequent film casting and solvent evaporation give a UN/PAA film which transforms to UN/PI and then RUN/PI via stepwise thermal treatment. b) Optical photographs of UN/PAA, UN/PI, and RUN/PI composite membranes after thermal treatment. The thickness of membranes were 20–30 μm.

dispersed in organic solvent is maintained before the critical gelation point is reached. Each particle in the sol is a type of nanogel consisting of a urea-bonded covalent network that forms via crosslinking polymerization of multi-functional monomers. The amine/isocyanate-to-urea conversion and the size of particles of the UN sols may be adjusted so that the blend of UN with a polymer can have a suitable morphological structure after phase-separation. In the present study, the UN sol to be mixed with the PAA solution was obtained by stirring the reactant solution for a sufficient time until the conversion approaches near 80%, which is the sol–gel transformation point of the monomer mixture.

We chose poly(amic acid) (PAA), a prepolymer of polyimide (PI), for blending with the UN sol to form a nanocomposite film. We anticipated that because the UN nanoparticles contained residual amine and isocyanate functional groups on their surfaces, the PAA chains which have carboxylic acid groups along their backbones could be easily adsorbed onto the UN particles via hydrogen bonding or electrostatic interactions. By optimizing the UN and PAA solution compositions, the sol state of the UN/PAA mixture could be prevented from forming macroscopic aggregates or gels. The process of preparing a microporous covalent-network nanocomposite membrane (Figure 1) was divided into three steps: 1) The UN sol and a PAA solution were mixed and then cast onto a substrate to produce a UN/PAA blend film; 2) the film was heated to imidize the PAA and obtain a dry UN/PI blend film; 3) the UN/PI film was then heated to rearrange the UN to form rearranged-UN (RUN), yielding a RUN/PI blend film. Thus, the UN sol was prepared in DMF by polymerizing tetrakis(4-aminophenyl)-methane (TAPM) and 1,6-hexamethylenediisocyanate (HDI), and then mixed with a solution of PAA prepared separately by polymerizing pyromellitic dianhydride (PMDA) and 4,4′-oxydianiline (ODA). Free-standing films with a thickness that could be controlled on the tens of micrometers scale were readily obtained after each of the three steps (Figure 1b).

Although the initial UN nanoparticles were aggregated to larger size by addition of PAA, the size of the aggregates was in the sub-micrometer range at a PAA weight fraction (W_p) smaller than 0.5, as indicated by the dynamic light scattering (DLS) results obtained from the mixed solution (Figure 2a and Figure S1 in the Supporting Information). Increasing the amount of PAA added to the UN sol increased the size of aggregates. PAA chains adsorbed initially to the surfaces of the UN particles via electrostatic interactions or through a reaction between the isocyanate and carboxylic acid groups. The adsorbed PAA chains may help the UN particles disperse in the solution; however, the addition of more PAA chains to the solution could cause aggregation driven by a depletion interaction.[17] Indeed, the solution

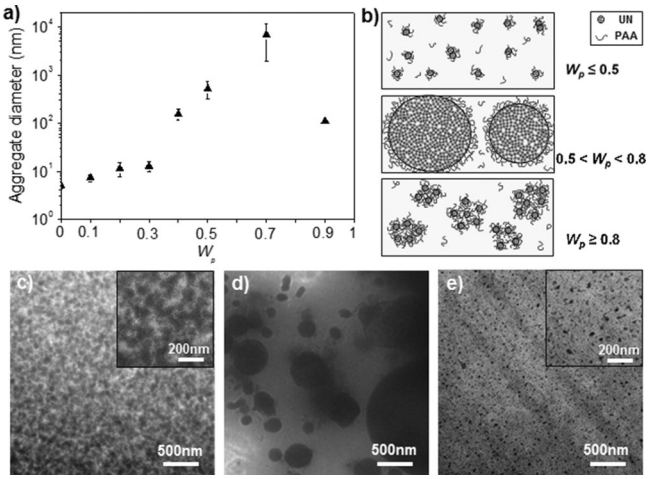

Figure 2. Preparation of the RUN/PI nanocomposite films from the UN/PAA sol mixtures. a) Plot of the average DLS-measured particle size in a mixture of the UN sol and the PAA solution, for various weight fractions of PAA (W_p). All mixed solutions were diluted with DMF to a solid content of 4 w/v% prior to collecting the DLS measurements. b) Schematic diagram showing the different UN/PAA aggregates formed in different ranges of W_p. c)–e) Cross-sectional TEM images of the final RUN/PI films obtained after treatment at $T_r = 270$°C at different values of W_p: c) $W_p = 0.4$, d) $W_p = 0.6$, and e) $W_p = 0.9$. Cross-sections 60 nm thick were obtained from the films using a microtome. RUN domains were stained with RuO_4 and appear dark.

prepared with W_p exceeding 0.6 became turbid, indicative of the formation of micron-sized aggregates (Figure 2b).

Nanoscale UN/PAA blends were obtained at $W_p \leq 0.5$ and provided transparent UN/PI films after imidization upon heating to 200 °C (Figure 1b). The FT-IR spectra (Figure S2) confirmed that PAA was completely imidized in the films. The RUN/PI films were then obtained by heating the UN/PI blend to a rearrangement temperature (T_r) between 200 and 270 °C at a rate of 2 °C min^{-1} and then keeping at T_r for 1 h. Microporous channels formed along the microdomains of the urea network (UN) in the blend film (Figure 1b) as discussed below.

Transmission electron microscopy (TEM) images of ultrathin sections of the RUN/PI composite films revealed that the morphology varied with the composition of the initial UN/PAA sol mixture. The films prepared from $W_p \leq 0.5$ exhibited three-dimensionally interconnected domain morphologies (Figure 2c). We found that the RUN domains in the PI matrix were selectively stained with RuO_4 whereas the UN and PI domains could not be distinguished by staining. AFM images of UN/PI film indicate that three-dimensionally separated domain morphology formed even before thermal treatment (Figure S7). The different activities of the RUN and UN to the staining agent enabled visualization of the RUN domain growth with increasing T_r (Figure S8); indeed, the data suggest that the RUN domains nucleated locally and then grew to continuous domains. It is likely that the UN to RUN transformation starts near the surface of UN domains and propagates to the entire network domains while forming interconnected microporous channels. Macroscopic aggregates of UN domains formed within the PI matrix at $0.5 < W_p < 0.8$ (Figure 2d), consistent with the DLS data obtained from the corresponding solution mixtures. The blend prepared at $W_p \geq 0.8$ was characterized by small isolated UN domains throughout (Figure 2e). These UN domains were much smaller than the DLS aggregate size in the solution of the corresponding compositions, most likely a result of the formation of large compound aggregates in solution, which consisted of multiple small UN/PAA aggregates (Figure 2b).

The tensile modulus and strength of the RUN/PI composite membranes increased with increasing PI composition (Figure S5). The tensile modulus of the composite film prepared with a 60 wt% PI was almost identical to that obtained from the pure PI film. The strains-at-break of all the blend films and the pure RUN film were similarly low at 1–2%, suggesting that they consisted of the same continuous RUN domains that could be broken at a small strain. High modulus of the PI matrix helps the fragile RUNs to maintain the domain connectivity throughout the membrane (membrane shown in Figure 1b).

FT-IR spectra of the UN/PI film and the RUN/PI films treated at different values of T_r revealed that the UN domains in the blend were efficiently rearranged to form the desired structure even at T_r well below 300 °C (Figure 3). Aliphatic C–H stretching modes at 3000–2850 cm^{-1} weakened significantly in the RUN/PI at $T_r > 250$ °C, indicating that the aliphatic

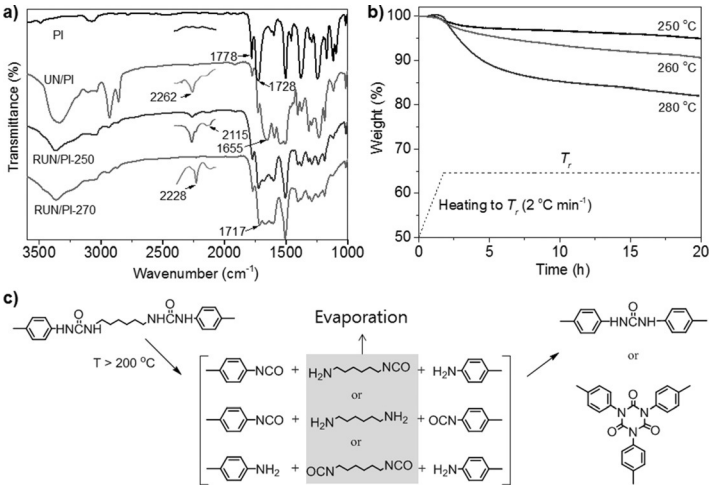

Figure 3. Rearrangement of UN to RUN in the nanocomposite blends. a) FT-IR spectra of the PI, UN/PI, and RUN/PI ($W_p = 0.1$). The "RUN/PI-250" and "RUN/PI-270" labels refer to the RUN/PI films treated at $T_r = 250$ and 270 °C, respectively. b) TGA data obtained at isothermal conditions at 250, 260, and 280 °C, respectively, using UN/PI ($W_p = 0.4$). Note that FT-IR spectra were obtained from the blend with a low PI content to better show the structural change of UN. c) Scheme of the thermal rearrangement of urea bonds.

segments were removed efficiently (Figure 3a). Isothermal TGA data (Figure 3b) showed weight losses close to the aliphatic content in the blend, although the rate of weight loss appeared to be slower in the TGA cell than in sample preparation furnace. The urea bonds underwent thermolysis, as indicated by the decrease in the urea C=O stretching band at 1655 cm^{-1} and the appearance of the isocyanate stretching mode at 2262 cm^{-1}. The carbodiimide (2115 cm^{-1}, N=C=N) and cyanamide (2228 cm^{-1}, C≡N stretch) peaks grew as the isocyanate peaks disappeared.[18] The formation of an isocyanurate ring was evident by the strengthened C=O stretching bands near 1717 cm^{-1}, which overlapped with the imide C=O stretching band. The RUN/PI displayed strong and broad N–H bands, indicating that the urea bonds reformed after expulsion of the aliphatic segments. The formation of isocyanurate nodes across the urea network should stabilize it against further thermal degradation. It should be noted that the volatiles were removed efficiently without generating macroscopic pinholes in the films, possibly because the three-dimensional continuous micropore channels facilitated the escape of vapors of small molecule fragments during thermal processing.

The films composed of UN/PAA, UN/PI, and RUN/PI, prepared at the three different stages of the thermal treatment (Figure 1b), were tested for gas transport. A dramatic increase in the permeability was observed in the RUN/PI films prepared at $T_r > 250$ °C, indicating that microporous channels were indeed generated by thermal treatment. RUN/PI-270 films exhibited N_2 or He permeability greater than 1000 Barrer. Because pure PI films did not exhibit a measurable permeability under the same conditions, the steep increase in the gas permeability must have been due to the thermally generated pores along the RUN domains.

The porosity characteristics (Figure 4a), estimated from the CO_2 adsorption isotherms obtained at 0 °C from the film

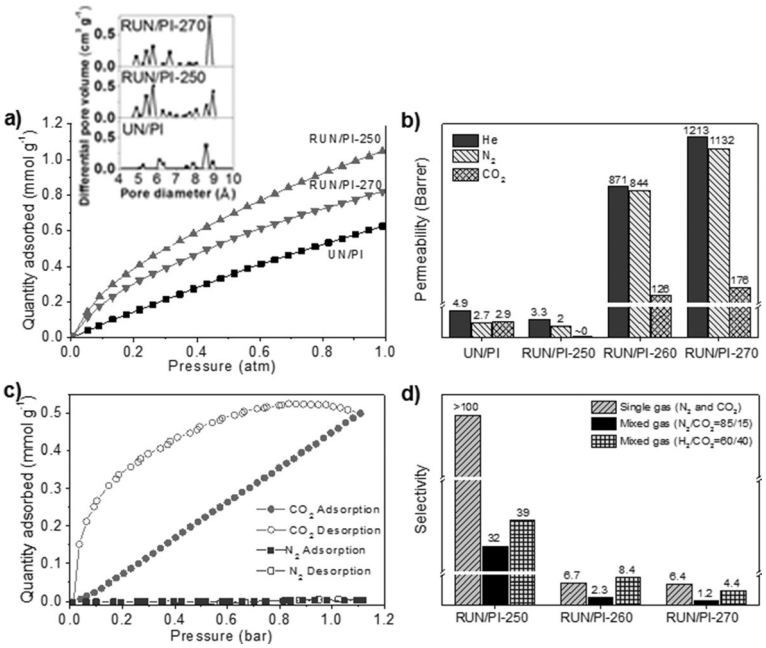

Figure 4. Porosity and gas permeability of the RUN/PI films as a function of the thermal rearrangement temperature. a) CO_2 adsorption isotherms for UN/PI, RUN/PI-250, and RUN/PI-270, respectively, acquired at 273 K. Inset: pore-size distribution derived from the CO_2 adsorption data on UN/PI, RUN/PI-250, and RUN/PI-270. b) Single gas permeability (He, N_2, and CO_2) of UN/PI, RUN/PI-250, RUN/PI-260, and RUN/PI-270. All films with thickness of 20–30 μm were prepared from the UN/PAA mixture with $W_p = 0.4$. The steady state flux was obtained after 10 h. c) Gas adsorption and desorption isotherm of a RUN/PI-250 film ($W_p = 0.4$) acquired at 298 K for CO_2 and N_2. d) The N_2/CO_2 selectivity and H_2/CO_2 selectivity of RUN/PI-250, RUN/PI-260, and RUN/PI-270 using single gas (CO_2 and N_2) and mixed-feed gases [N_2/CO_2 (85/15) and H_2/CO_2 (60/40)].

samples at different stages, indicated that micropores were indeed generated in situ through the RUN. With increasing T_r above 250 °C, the volume of micropores near 1 nm increased. While attempted TEM imaging of the composite film did not give data with discernible features at a few nanometer length scale (Figure S8), the TEM of a pure RUN sample treated at $T_r = 270$ °C exhibited a thread-like texture which was absent in the corresponding UN sample (See supporting information, Figure S9), indicating the microporous channels formed in the RUN at 270 °C. These data agree well with the permeability enhancement in the RUN/PI samples.

Intriguingly, the RUN/PI composite membranes exhibited reverse-selective separation behavior and were more permeable to N_2 while less permeable to CO_2 (Figure 4b). RUN/PI-250 films showed N_2/CO_2 separation factor greater than 30 even for a N_2/CO_2 (85/15) mixed feed gas (Figure 4d). The reverse-selectivity and permeability maintained constant values once a steady state was attained (Figure S11). Because only a small amount of CO_2 is needed for saturation of the surface inside the thin membrane, the result indicates that the reversed selectivity is not a direct consequence of preferential CO_2 adsorption onto the pore surface. The high reverse selectivity of the RUN/PI composite membranes could be accounted for by referring to the CO_2 and N_2 adsorption/desorption isotherms of the membranes, measured at room temperature (Figure 4c). The membranes exhibited a very high degree of hysteresis during CO_2 adsorption and desorption. The low-pressure desorption of CO_2 molecules proceeded slowly compared with the low-pressure adsorption process. By contrast, N_2 adsorption onto the membranes at room temperature was negligible.

The adsorption/desorption hysteresis is likely caused by the relatively large heat of adsorption of the RUN toward CO_2, which was 35–45 kJ mol^{-1} as estimated from their adsorption isotherms at different temperatures. The high heat of adsorption should prohibit CO_2 diffusion along the inner surface of microporous channels whereas N_2 diffusion was not hindered. With increasing the pore width by increasing T_r, Knudsen diffusion should override the surface diffusion mechanism, reducing the difference in permeability.

It should be noted that the RUN/PI-250 membranes, rejecting CO_2 nearly completely, transmitted He or N_2 only at low permeability values. The low permeability may be overcome by increasing T_r. For example, the RUN/PI-270 showed N_2 permeability of 1132 Barrer with N_2/CO_2 selectivity of 6.4. Although the selectivity decreased when a mixed gas of 15:85 CO_2/N_2 composition was used for the test, a significant level of reverse-selectivity was still observed in the membranes prepared at lower thermal conditions. Optimum performance with balanced selectivity and permeability may be achieved by modifying the processing conditions for rearranging UN to RUN in the blends, as shown by the preliminary results (Figure S12). The sample prepared with W_p of 0.4 exhibited higher N_2/CO_2 selectivity than those with $W_p = 0.3$ or 0.5. When treated isothermally for 1 h, the sample prepared at T_r near 250 °C showed higher selectivity than those prepared at higher T_r.

CO_2 permeates many polymeric membranes faster than N_2 because CO_2 is more soluble in the polymers than N_2 and has smaller kinetic diameter (3.3 Å) compared to N_2 (3.6 Å). Only a few organic/inorganic hybrid membrane systems display reverse CO_2/N_2 selective separation.[19] A key feature of such reverse-selective membranes is that they are made of mesoporous inorganic structures coated with CO_2-attractive organic matter. Our study results and the previous ones suggest that porous morphological structure functionalized with the groups interacting with a specific molecule can reject the transport of the molecule while transmitting non-interactive species. For carbon dioxide capture, the membranes exhibiting reverse-selective permeability have been suggested to be advantageous considering that CO_2 is automatically compressed in the feed side of the reverse-selective membrane, whereas the CO_2 permeated through a normal selective membrane would need to be compressed.[20] It is also possible to envisage that the reverse selective membranes are utilized for enriching a gas mixture with CO_2 by removing other gases from it which is then selectively separated by a normal selective membrane. How or where to use the reverse-selectivity membranes for practical applications must

be decided and justified with the economical calculations based on appropriate engineering parameters.

In summary, we successfully synthesized a microporous covalent network membrane derived from co-continuous blends of a porogenic urea network and a polyimide. We showed that the urea-based networks in the PI matrix could be transformed thermally while selectively expelling small molecular fragments to form a new network with reticular microporous molecular pathways that exhibited a high permeability to gas molecules. The resultant membranes exhibited reverse-selective separation behaviors toward CO_2/N_2 mixtures, blocking CO_2 while transporting N_2. The reverse selectivity may also be potentially useful for separation of other CO_2-containing gas mixtures including gases that may not interact with the membrane. The facile preparation of microporous membranes from a porogenic network/polymer blend film via in situ pore generation shows promise for the creation of new materials that enable advanced membrane-based technologies.

Experimental Section

Synthesis of UN: The 0.04 g mL^{-1} TAPM/HDI solution was prepared by dissolving TAPM (0.482 g, 1.263 mmol) in DMF (22.6 mL). HDI (0.425 g 2.527 mmol) was added to the solution and the mixture was stirred for 72 h at room temperature under nitrogen.

Synthesis of PAA: a 0.15 g mL^{-1} PAA solution was prepared with ODA and PMDA. PMDA (1.0906 g, 0.005 mol) was added to a DMAc (dimethylacetamide) solution (13.95 mL) containing an equimolar amount of ODA (1.0012 g, 0.005 mol). The ODA/PMDA mixture was stirred at room temperature for 3 h under nitrogen, and a viscous PAA solution was obtained.

Preparation of the UN/PI nanocomposite: The UN/PI nanocomposite was prepared by blending the UN sol and PAA. PAA was added to the UN sol in various weight fractions of the polymer (W_p) over the range 0.1–0.9. The solution mixture was stirred for 30 min. The resulting UN/PAA mixture was cast onto on a glass plate and subsequently dried and imidized at 60 °C for 2 h, 100 °C for 1 h, and 200 °C for 1 h under nitrogen.

Preparation of the RUN/PI nanocomposite membrane: RUN/PI films were synthesized by thermal treatment of UN/PI. The UN/PI film was heated to the desired temperature (230–270 °C) in an electric furnace at a heating rate of 2 °C min^{-1} under nitrogen. The sample was held at this final temperature (T_r) for 1 h. After cooling, the sample was removed from the furnace. The glass plate supporting the film was immersed in water to obtain a free-standing RUN/PI film and was then dried in a vacuum oven at 100 °C for 12 h.

Acknowledgements

This work was supported by a Korea CCS R&D Center (KCRC) grant, and funded by the Korean Government (Ministry of Science, ICT & Future Planning) (NRF-2014M1A8A1049265).

Keywords: covalent networks · membranes · microporous materials · organic sol–gel synthesis · reverse-selective separation

How to cite: *Angew. Chem. Int. Ed.* **2016**, *55*, 1318–1323
Angew. Chem. **2016**, *128*, 1340–1345

[1] a) J. Weber, Q. B. Meng, *Encyclopedia of Polymer Science and Technology*, Wiley, New York, **2002**; b) M. Kim, M. Byeon, J.-S. Bae, S.-Y. Moon, G. Yu, K. Shin, F. Basarir, T.-H. Yoon, J.-W. Park, *Macromolecules* **2011**, *44*, 7092–7095; c) W. Jens, T. Arne, *Nanoporous Materials*, CRC, Boca Ration, **2013**, pp. 1–42.

[2] a) A. K. Sekizkardes, T. Islamoglu, Z. Kahveci, H. M. El-Kaderi, *J. Mater. Chem. A* **2014**, *2*, 12492–12500; b) Q. Zhang, Y. Yang, S. Zhang, *Chem. Eur. J.* **2013**, *19*, 10024–10029; c) J. Wang, S. Xu, Y. Wang, R. Cai, C. Lv, W. Qiao, D. Long, L. Ling, *RSC Adv.* **2014**, *4*, 16224–16232.

[3] a) Y. Zhang, S. N. Riduan, *Chem. Soc. Rev.* **2012**, *41*, 2083–2094; b) L. Zou, D. Feng, T.-F. Liu, Y.-P. Chen, S. Fordham, S. Yuan, J. Tian, H.-C. Zhou, *Chem. Commun.* **2015**, *51*, 4005–4008; c) P. Zhang, Z. Weng, J. Guo, C. Wang, *Chem. Mater.* **2011**, *23*, 5243–5249.

[4] C. E. Chan-Thaw, A. Villa, P. Katekomol, D. Su, A. Thomas, L. Prati, *Nano Lett.* **2010**, *10*, 537–541.

[5] a) A. P. Côté, A. I. Benin, N. W. Ockwig, M. O'Keeffe, A. J. Matzger, O. M. Yaghi, *Science* **2005**, *310*, 1166–1170; b) S.-Y. Ding, W. Wang, *Chem. Soc. Rev.* **2013**, *42*, 548–568.

[6] A. Corma, H. García, F. X. Llabrés i Xamena, *Chem. Rev.* **2010**, *110*, 4606–4655.

[7] N. B. McKeown, P. M. Budd, *Chem. Soc. Rev.* **2006**, *35*, 675–683.

[8] D. Yuan, W. Lu, D. Zhao, H.-C. Zhou, *Adv. Mater.* **2011**, *23*, 3723–3725.

[9] a) Y. Xu, S. Jin, H. Xu, A. Nagai, D. Jiang, *Chem. Soc. Rev.* **2013**, *42*, 8012–8031; b) A. Patra, J.-M. Koenen, U. Scherf, *Chem. Commun.* **2011**, *47*, 9612–9614; c) C. Gu, N. Huang, J. Gao, F. Xu, Y. Xu, D. Jiang, *Angew. Chem. Int. Ed.* **2014**, *53*, 4850–4855; *Angew. Chem.* **2014**, *126*, 4950–4955.

[10] S. Yao, X. Yang, M. Yu, Y. Zhang, J.-X. Jiang, *J. Mater. Chem. A* **2014**, *2*, 8054–8059.

[11] M. G. Schwab, D. Crespy, X. Feng, K. Landfester, K. Müllen, *Macromol. Rapid Commun.* **2011**, *32*, 1798–1803.

[12] a) S.-Y. Moon, J.-S. Bae, E. Jeon, J.-W. Park, *Angew. Chem. Int. Ed.* **2010**, *49*, 9504–9508; *Angew. Chem.* **2010**, *122*, 9694–9698; b) S.-Y. Moon, E. Jeon, J.-S. Bae, M. Byeon, J.-W. Park, *Polym. Chem.* **2014**, *5*, 1124–1131; c) S.-Y. Moon, H.-R. Mo, M.-K. Ahn, J.-S. Bae, E. Jeon, J.-W. Park, *J. Polym. Sci. Part A* **2013**, *51*, 1758–1766; d) X. Zhu, C. Tian, S. M. Mahurin, S.-H. Chai, C. Wang, S. Brown, G. M. Veith, H. Luo, H. Liu, S. Dai, *J. Am. Chem. Soc.* **2012**, *134*, 10478–10484.

[13] a) Y. Yoo, Z. Lai, H.-K. Jeong, *Microporous Mesoporous Mater.* **2009**, *123*, 100–106; b) Y.-S. Li, F.-Y. Liang, H. Bux, A. Feldhoff, W.-S. Yang, J. Caro, *Angew. Chem. Int. Ed.* **2010**, *49*, 548–551; *Angew. Chem.* **2010**, *122*, 558–561.

[14] a) D. Bastani, N. Esmaeili, M. Asadollahi, *J. Ind. Eng. Chem.* **2013**, *19*, 375–393; b) S. R. Venna, M. Lartey, T. Li, A. Spore, S. Kumar, H. B. Nulwala, D. R. Luebke, N. L. Rosi, E. Albenze, *J. Mater. Chem. A* **2015**, *3*, 5014–5022; c) M. A. Aroon, A. F. Ismail, T. Matsuura, M. M. Montazer-Rahmati, *Sep. Purif. Technol.* **2010**, *75*, 229–242; d) A. F. Bushell, P. M. Budd, M. P. Attfield, J. T. A. Jones, T. Hasell, A. I. Cooper, P. Bernardo, F. Bazzarelli, G. Clarizia, J. C. Jansen, *Angew. Chem. Int. Ed.* **2013**, *52*, 1253–1256; *Angew. Chem.* **2013**, *125*, 1291–1294.

[15] a) S. Caruso, S. Foti, P. Maravigna, G. Montaudo, *J. Polym. Sci. Polym. Chem. Ed.* **1982**, *20*, 1685–1696; b) E. Delebecq, J.-P. Pascault, B. Boutevin, F. Ganachaud, *Chem. Rev.* **2012**, *112-112*, 80–118.

[16] S.-Y. Moon, E. Jeon, J.-S. Bae, M.-K. Park, C. Kim, D. Y. Noh, E. Lee, J.-W. Park, *J. Mater. Chem. A* **2015**, *3*, 14871–14875.

[17] P. J. Lu, E. Zaccarelli, F. Ciulla, A. B. Schofield, F. Sciortino, D. A. Weitz, *Nature* **2008**, *453*, 499–503.

[18] a) E. Delebecq, J.-P. Pascault, B. Boutevin, F. Ganachaud, *Chem. Rev.* **2013**, *113*, 80–118; b) H. G. Khorana, *Chem. Rev.* **1953**, *53*,

145 – 166; c) W. C. Schneider, *J. Am. Chem. Soc.* **1950**, *72*, 761 – 763.

[19] a) P. Kumar, S. Kim, J. Ida, V. V. Guliants, *Ind. Eng. Chem. Res.* **2008**, *47*, 201 – 208; b) C. Zhang, Y. Xiao, D. Liu, Q. Yang, C. Zhong, *Chem. Commun.* **2013**, *49*, 600 – 602; c) G. Xu, J. Yao, K. Wang, L. He, P. A. Webley, C.-s. Chen, H. Wang, *J. Membr. Sci.* **2011**, *385 – 386*, 187 – 193.

[20] a) E. Favre, D. Roizard, R. Bounaceur, W. J. Koros, *Ind. Eng. Chem. Res.* **2009**, *48*, 3700 – 3701; b) R. Bounaceur, N. Lape, D. Roizard, C. Vallieres, E. Favre, *Energy* **2006**, *31*, 2556 – 2570.

Received: September 7, 2015
Published online: December 9, 2015

